IEEE Access
Multidisciplinary ⋮ Rapid Review ⋮ Open Access Journal

Received August 9, 2021, accepted August 17, 2021, date of publication August 24, 2021, date of current version September 21, 2021.

Digital Object Identifier 10.1109/ACCESS.2021.3106959

Ultra-Thin Broadband Transmission FSS for Linear Polarization Rotation

NICKOLAS M. LITTMAN[1], (Student Member, IEEE), STEVEN G. O'KEEFE[1], AMIR GALEHDAR[2], (Member, IEEE), HUGO G. ESPINOSA[1], (Senior Member, IEEE), AND DAVID V. THIEL[1], (Life Senior Member, IEEE)

[1]School of Engineering and Built Environment, Griffith University, Brisbane, QLD 4111, Australia
[2]Defence Science and Technology Group, Melbourne, VIC 3207, Australia

Corresponding author: Nickolas M. Littman (n.littman@griffith.edu.au)

This work was supported by the Defence Science and Technology Group (DSTG), Australia.

ABSTRACT Frequency-selective surfaces (FSSs), have various applications in microwave electromagnetics. This paper reports a solution to the current FSS challenges of flexibly, low profile, simple fabrication and polarization control using a novel structure operating across X and Ku frequency bands where a linearly polarized wave is rotated by 90°. The FSSs were fabricated by laser engraving a thin layer of 5μm aluminum on a 65 μm Mylar substrate with a relative permittivity of 2.7, and separated by a dielectric spacing layer of 0.9 mm polypropylene substrate, with a relative permittivity of 3. The co and cross-polarized reflection and transmission response of the structure was investigated using numerical modeling and was measured experimentally. A parametric study was also conducted focusing on key performance indicators, and specifically the bandwidth of the structure. The novelty of this polarization rotation structure lies in its ultra-thin profile (0.034 λ_0), flexibility and significant transmission bandwidth. The fabricated prototypes experimental results were in good agreement with the simulated results, with a simulated −6 dB bandwidth of 61% and a measured −6dB bandwidth of 60%. Applications include antenna radomes where polarization is particularly important, as well as other polarization filtering applications which require a conformal low profile structure.

INDEX TERMS Flexible, frequency selective surface (FSS), microwave filters, polarizer, ultra-thin.

I. INTRODUCTION

Frequency Selective Surfaces (FSSs) have unique electromagnetic properties. FSSs are periodic arrays comprised of conductive elements supported by a dielectric substrate, where the geometry of the elements govern its frequency response [1]. These surfaces allow for isolation, absorption and/or filtering in microwave and optical applications [2].

One such use of FSS is polarization rotation, often used in polarization separation applications such as radiometers and imaging radars as well as satellite communications [3]. Polarization rotating structures can be classified as either reflection type or transmission type depending on the direction of the manipulated wave. Split ring [4] as well as other types of patch and grid FSSs [5]–[7] have been cascaded in front of a ground plane to produce reflection type polarizations. Several designs for transmission polarization rotation have been investigated, based on quarter-wave slots [8] and Substrate Integrated Waveguide (SIW) designs [9]. These SIW polarization rotators use cavities to couple energy between slots in the arrays, and are limited by their rigidity and thicknesses which are around 0.1 λ_0 − 0.2 λ_0 [9]–[13].

Multi-layered designs, consisting of cascaded FSS and dielectric spacing layers have also been explored, where broad bandwidths have been reported, however, the profile of these structures are quite large, and consequently limits its practical applications [14]. Many FSS geometries for polarization selection have been proposed including crossed-dipole [8], [15], [16], patches [17], [18], slots [7], [19], meanderlines [20], as well as three-dimensional (3-D) structures [21], [22]. Notably, slot types can be used to create either transmission or reflection polarizers using multiple layers.

In this study, a macro structure of co planar meandered slots of connected half wavelength slot elements are presented. The specific design of the structure of orthogonally positioned FSSs was optimized to via modelling the

The associate editor coordinating the review of this manuscript and approving it for publication was Xiu Yin Zhang.

structures frequency responses as a function of the main parameters consisting of element width, element length and separation distance. The objective of this study was to minimize the profile and to maximize the bandwidth whilst maintaining other key performance indicators of angular stability, co-polarized reflection bandwidth. The proposed design offers improvements over existing designs including its increased fractional operational bandwidth, conformal nature and low profile.

A novel laser engraving fabrication technique was utilized to create the FSSs and provides several key advantages over existing techniques such as the ability to create thin, flexible prototypes of arbitrary topology [23]. This process enables the creation of large conductive arrays which can be used in both single layered samples or incorporated into complex multi-layered structures.

II. POLARIZATION ROTATOR DEISGN

The slot type elements were arranged in a square grid lattice, with constant inter-element spacing in both the x and y axis. The unit cell is illustrated in Fig. 1, where the element or slot width was maximized to increase the bandwidth of the structure, whilst maintaining the slot geometry.

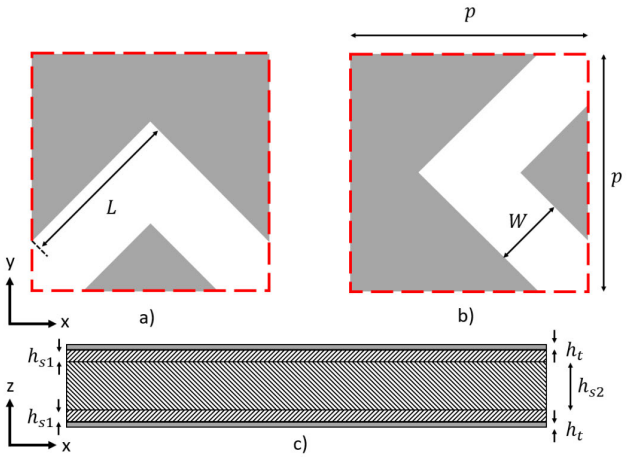

FIGURE 1. Polarization rotating FSS unit cells with periodicity, p, element lengths, l_1 and l_2 with element width w: (a) Top view of the top layer unit cell geometry, (b) Top view of the bottom layer unit cell geometry and (c) Cross sectional view showing the layers, the conductive track height, h_t, the substrate thickness, h_{s1}, and the spacer thickness, h_{s2}.

Because of this, the FSS layers can be considered as a macro structure of connected slots, where the surface can then be seen as collinear arrays of meandered slots. This structure can be explained using mode coupling theory where the structure is analogous to an aperture-waveguide-aperture structure, where the electric fields are perpendicular to the slots.

The resonant frequency depends on the slot length within the unit cell, which should be approximately a half wavelength. The resonant frequency can be approximated as

$$f_r \cong \frac{c_0}{2l_s\sqrt{\varepsilon_{eff}}} \tag{1}$$

where, c_0 is the speed of light in a vacuum, l_s is the length of the slot, and ε_{eff} is the effective permittivity of the dielectric.

The top FSS layer is an array of meandered slots, as illustrated in Fig. 1a. The slot selects from the incident radiation through the alignment of the fields due to its orientation. The radiation then propagates through the dielectric substrate layer before reaching the bottom FSS layer. This bottom FSS is also an array of meandered slots, as illustrated in Fig. 1b, where a polarization is again selected due to the slots geometry. The coupling will take place where the slots overlap. In this configuration with a meandered horizontal top layer and meandered vertical bottom layer, the coupling occurs where half of the top and bottom layer slots overlap due to the meandering. Thus, a signal received on the top layer will be coupled into the bottom layer and reradiated with a polarization twisted by 90°.

Due to the different orientations of the top and bottom FSS layers, they select and reradiate different polarizations, with the top layer selecting linear Y-polarization and the bottom layer selecting linear X-polarization. The selection of orientation of the slots can be modified to create X to Y polarization rotation by arranging the unit cell in Fig. 1b as the top FSS and the unit cell in Fig. 1a as the bottom FSS. Similarly, a filter can also be created by selecting two FSS layers of the same orientation which will transmit a single polarization (X to X-polarization or Y to Y-polarization) and reflect another polarization without rotation. The phase of the rotated wave depends on the direction of rotation between layers, where a polarizer with the bottom FSS having a clockwise rotation with respect to the top layer will be out of phase in comparison to an anticlockwise rotation.

The proposed structure is comprised of 3 layers; the top and bottom FSS which are each comprised of a conductive layer and dielectric substrate, as well as the dielectric spacer, separating the two FSS as illustrated in Fig. 1c. The top FSS layer, comprised a 5 μm aluminum sheet with a conductivity 5×10^4 S/m and a 65 μm supporting Mylar substrate with a relative permittivity of 2.7. Similarly, the bottom FSS layer, is identical to the top layer FSS, with a 90° rotation in the z axis. The dielectric spacer is a 0.9 mm thick, semi-transparent polypropylene sheet with a relative permittivity similar to the Mylar substrate.

The design parameters of the structure are outlined in Table 1. These values were chosen to maximize bandwidth whilst maintaining reasonable frequency performance. Consideration was also taken to allow for enough unit cells to be measured in the sample size, ensuring the simulation is accurate for an infinite plane, and to function in the usable frequency range of microwave antennas used in experimental measurements.

A laser engraver (Trotec, Speedy 360) was used to fabricate a 330 mm × 330 mm prototype sheet consisting of a 33 × 33 periodic array of elements as shown in Fig. 2. The laser engraver was used to remove the aluminum whilst leaving the Mylar substrate to create the slot elements with high resolution [23]. A polypropylene dielectric separation

TABLE 1. Physical parameters of designed FSS polarizer.

Symbol	DESCRIPTION	Dimension
p	Unit cell size	9.9 mm
l_1	Element outer length	7 mm
l_2	Element inner length	4 mm
w	Element width	3 mm
h_t	Conductor height	0.005 mm
h_{s1}	Substrate height	0.065 mm
h_{s2}	Spacer height	0.900 mm
ε_{r1}	Substrate relative permittivity	2.7
ε_{r2}	Spacer relative permittivity	3
σ	Conductivity	5×10^4 S/m

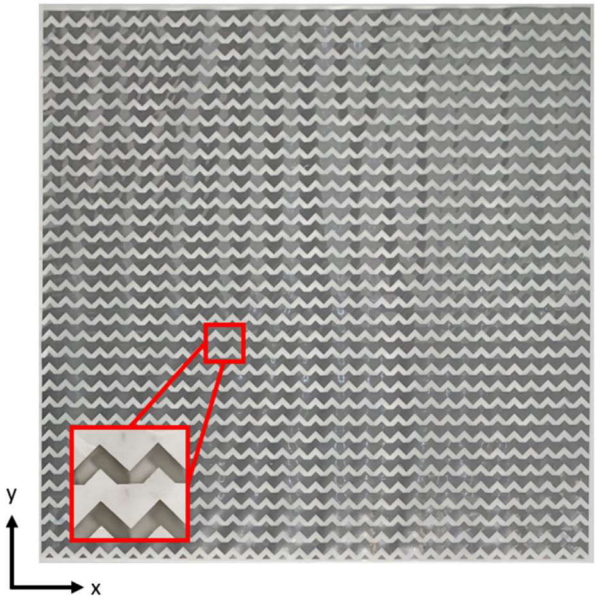

FIGURE 2. Fabricated polarization rotating FSS 330 mm × 330 mm prototype crated using a laser engraving fabrication technique, with a 9.9 mm unit cell.

layer was then inserted between the FSSs sheets, ensuring the slots were properly aligned, so that half of each slot on the top layer overlaps with half of the corresponding slot on the rotated bottom layer, as seen in the zoomed unit cells of Fig. 2.

III. POLARIZATION ROTATOR MODELLING

The structure was modelled using CST Microwave Studio® (www.3ds.com). The co-and cross-polarized reflection (S_{11}) along with the co-and cross-polarized transmission responses (S_{12}) were calculated in the frequency range of 4-16 GHz. Unit cell boundary conditions were applied in both the x and y axis. A linearly polarized plane wave propagating normal to the surface (along the z axis), with the electric field vector in the x axis was used to illuminate the structure. The main design parameters are explored along with their influence on key performance indicators of the structure, where a single parameter was varied with all other parameters remaining constant as summarized in table 1.

The simulated frequency response of the designed structure is shown in Fig. 3, with cross-polarized transmission being

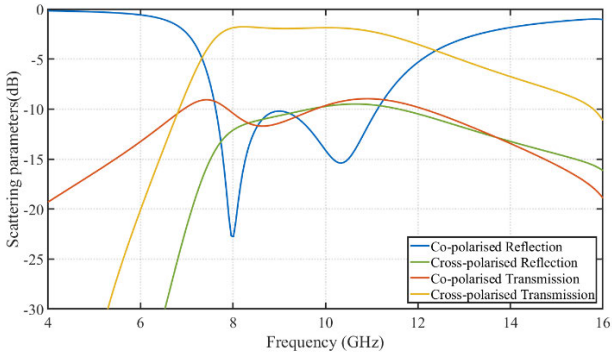

FIGURE 3. Simulated frequency response of the designed FSS polarization rotator.

significantly higher in comparison to the other measured responses across the operating range. The cross-polarized transmission is −2 dB between approximately 8 GHz and 11 GHz, where rotation functionality occurs. In contrast, the co-polarized transmission is effectively blocked across this range. Similarly, both the co- and cross-polarized reflection is significantly lower at around −10 dB at these frequencies. The co-polarized reflection response shows two distinct resonances at 8 GHz and 10.3 GHz due to the two FSS layers. The first resonance is due to the individual aperture (unit cell), whilst the second resonance is due to the coupling of apertures.

The E-fields at the edge of the conductive FSS layers at 8 GHz are shown in Fig. 4. The direction of the fields point inwards on the top layer as seen in Fig. 4a, and are opposite to that seen in the bottom layer in Fig. 4b, where the fields point outwards with respect to the slot. The induced magnetic surface currents can be obtained using the E-field direction using the surface equivalence principle [25]. In this case, the magnetic current distribution is along the z-direction in the top layer and along the $-z$-direction in the bottom layer, corresponding to the received Y-polarisation in the top layer and the transmitted Y-Polarisation in the bottom.

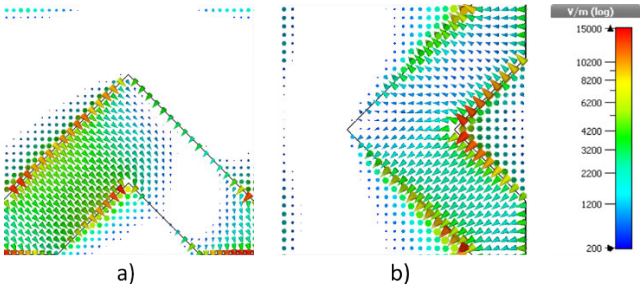

FIGURE 4. Simulated electric field distribution at 8 GHz for the a) top layer and b) bottom layer.

Similarly, at 10.3 GHz, the fields point inwards at the edge of the top FSS, as seen in Fig. 5.a and outwards at the edge of the bottom FSS, as seen in Fig. 5b, as well as a shift in distribution due to the additional coupling effects.

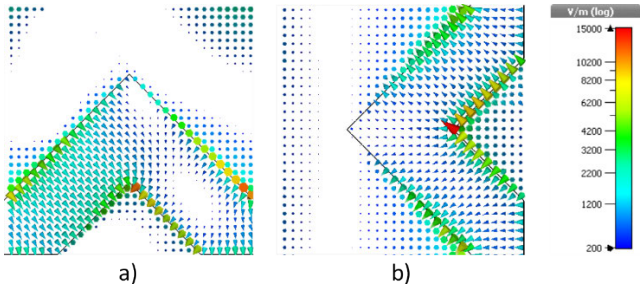

FIGURE 5. Simulated electric field distribution at 10.3 GHz for the a) top layer, b) bottom layer.

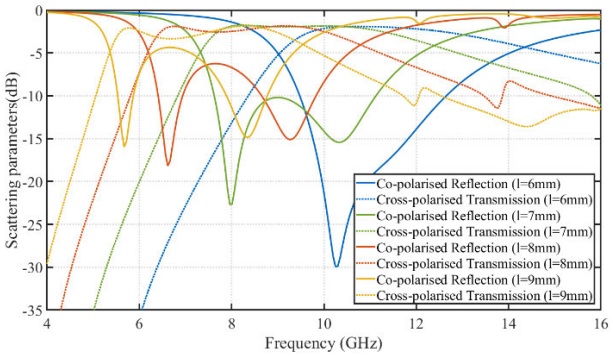

FIGURE 6. Simulated co-polarized reflection and cross-polarization transmission response with varying element length, *l*, displaying a decrease in resonant frequency.

A. EFFECT OF ELEMENT LENGTH

A frequency shift downwards in both the co-polarized reflection and cross-polarized transmission is visible with an increase in element length, l, as shown in Fig. 6.

This is due to the resonant nature of the slot elements which are approximately a half wavelength and therefore are inversely proportional to the frequency. When the element length is 9 mm, two distinct nulls with similar magnitudes are evident in the co-polarized reflection at 5.6 GHz and 8.3 GHz. As the element length is reduced, the frequency of operation is shifted upwards, with a noticeable reduction in the magnitude of the second null as the two nulls shift closer together, resulting in a more uniform cross-polarized transmission response. When the element length is 6mm, the second null at the higher frequency has almost completely merged with the first null at 10.3 GHz. The percentage bandwidth of this structure is unaffected by varying element lengths. This is further supported in the cross-polarized where an increased element length also reduces the resonant frequency with minimal differences in the percentage bandwidth.

B. EFFECT OF ELEMENT WIDTH

The influence of the element width, w, on the co-polarized reflection and cross-polarized transmission response is shown in Fig. 7. The resonant frequency increases with an increase in element width. Similarly, the bandwidth also increases with the narrowest element with a width of 1mm having a -6 dB cross-polarised transmision bandwidths of 47%, 57%,

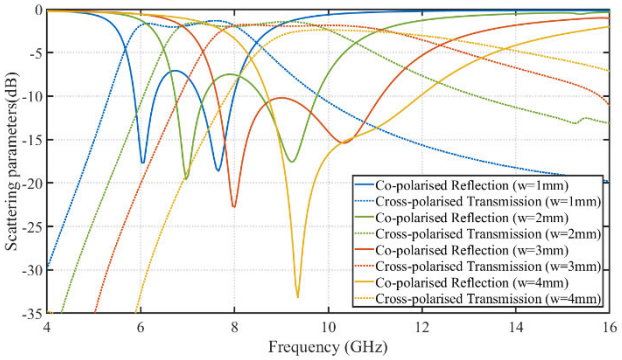

FIGURE 7. Simulated co-polarized reflection and cross-polarization transmission response with varying element width, *w*, displaying a shift in frequency and bandwidth.

61% and 58% for widths of 1 mm, 2 mm, 3 mm and 4 mm respectively. The bandwidth of the 4 mm slot width is less than the bandwidth of the 3 mm slot due to the two resonances converging, as evident in the co-polarised transmission. It is notable, that a narrow width adversely effects the co-polarised transmission resulting in magnitudes ranging between -5 dB and -10 dB across the operating frequencies as the two resonances, resulting in significant reflection across the operating frequencies. The width is proportional to the structures bandwidth, but can compromise other performance features.

C. EFFECT OF SEPERATION DISTANCE

The dielectric spacing affects both the operating frequency range and bandwidth of the structure as seen in Fig. 8, where the total separation distance, h, is the combined height of the two Mylar substrates, h_{s1}, as well as the Polypropylene spacer h_{s1}. When the separation between conductive FSS is small, such as when the spacing is 0.3 mm, where the co-polarized reflection magnitudes do not fall below -10 dB and possess two distinct resonances which are very far apart. As the spacing is increased, the two nulls merge and possess greatly reduced co-polarized reflection. At the greatest spacing of 1.2 mm, the two co-polarized reflection nulls merge and the cross-polarized transmission bandwidth is reduced. This is reflected in the cross-polarized transmission, which is significantly reduced with smaller spacing's typically ranging between -4 dB and -6 dB across the operating range, whilst greater spacing's possess a flatter response at -2 dB with reduced bandwidths. Therefore an intermediate spacing will result in better performance, as the reflection can be reduced to below -10 dB whilst maintaining an acceptable transmission loss.

D. EFFECT OF CONDUCTIVITY

The conductivity, σ, effects the bandwidth and magnitude at resonance as well as introduces a slight frequency shift as seen in Fig. 9. The -10 dB co-polarized reflection bandwidths 24.4%, 37.7%, 36.6% 36.4% along with -6dB transmission bandwidths 56.9% 61.1% 61.9% 62% for the respective conductivities. Therefore a lower conductivity will

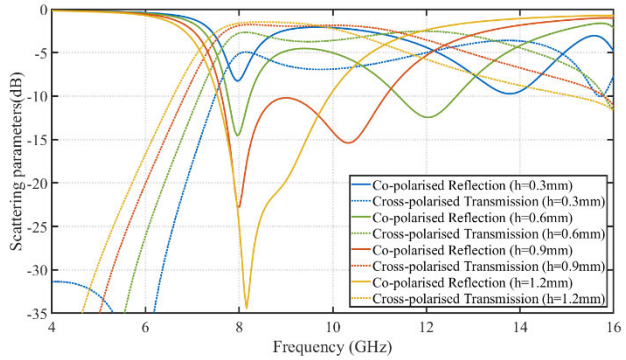

FIGURE 8. Simulated co-polarized reflection and cross-polarization transmission response with varying separation distance, *h*, displaying a change in bandwidth.

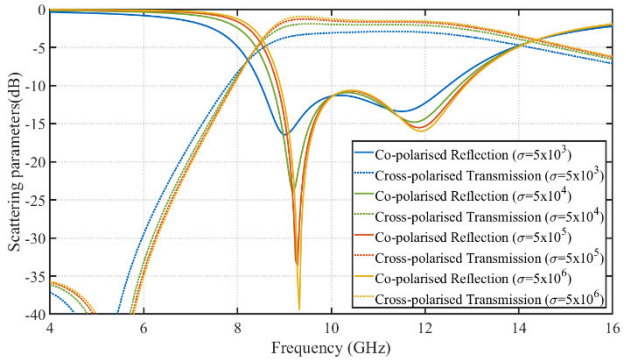

FIGURE 9. Simulated co-polarized reflection and cross-polarized transmission with varying conductivity, σ, displaying an increase in cross-polarised transmission.

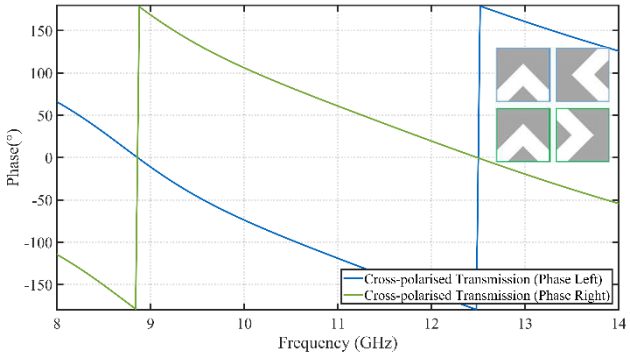

FIGURE 10. Simulated cross-polarized transmission phase with varying z axis rotation between layers.

generally result in an increased rejection bandwidth and a greater conductivity will result in an increased transmission bandwidth. Notably, the transmission bandwidth is notably less sensitive to conductivity, however this significantly impact the transmitted magnitude, where the average values range between -4 dB to -1.5 dB for the conductivities. The change in cross-polarised transmission is due to the change in conductive losses experienced by the currents circulating around the elements. In this case, the conductive layer on top of the substrate is very thin and thus has a finite conductance, however a thicker or more conductive metal layer will reduce

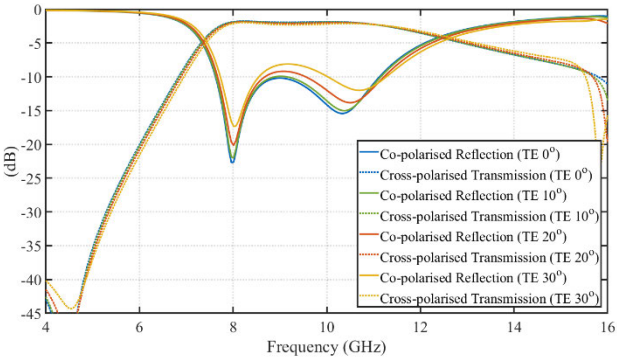

FIGURE 11. Simulated TE co-polarized reflection and cross-polarized transmission for different incident angles.

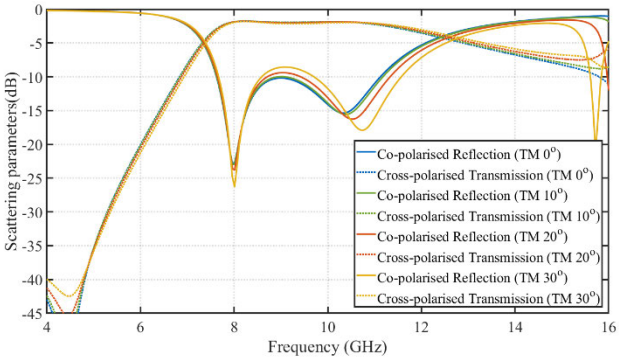

FIGURE 12. Simulated TM co-polarized reflection and cross-polarized transmission for different incident angles.

loss. A frequency shift of approximately 3.5% is evident when comparing the highest and lowest conductivities.

E. EFFECT OF ROTATION BETWEEN LAYERS

The rotation between the FSS layers determines the phase of the transmitted wave. This is seen in Fig. 10, where the transmitted waves of a structure with a 90° rotation in the z axis (clockwise/left) and a structure with a $-90°$ rotation in the z axis (anti-clockwise/right) are 180° out of phase.

F. EFFECT OF ANGLE OF INCIDENCE

The cross-polarized transmission of the structure under varying transverse electric (TE) and transverse magnetic (TM) angles of incidence as shown in Fig. 11 and Fig. 12 respectively. The co-polarized refection of the structure is more sensitive to oblique angles of incidence in comparison to the cross-polarized transmission.

The frequency shift when comparing normal incidence to oblique angles of incidence is minor for both TE and TM. For TE, the structure exhibits co-polarized reflection stability below to 20°, where the bandwidth is stable, with a reduction reflection magnitude and frequency shift of 3.5% for the second resonance at 30°. Similarly, the cross-polarized transmission is slightly affected with an approximately a 1dB difference between 0° and 30°.

In the TM mode, the angle of incidence, the co-polarized reflection is also stable below 20° with a slightly increase

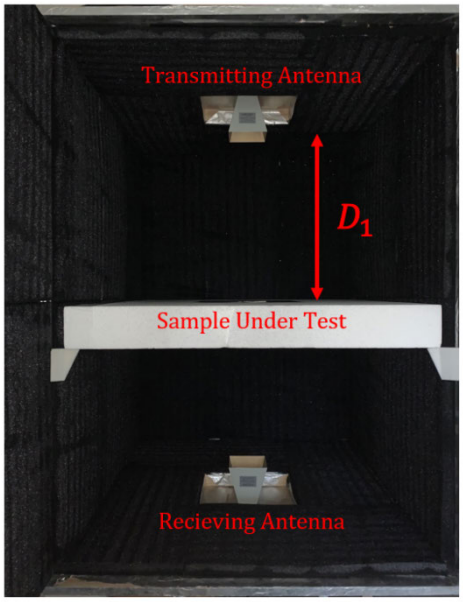

FIGURE 13. The experimental setup showing the sample under test suspended between two horn antennas separated by distance, D_1, inside a microwave anechoic chamber.

bandwidth due to the deepening of the resonances. The cross polarized transmission is very stable across all of the simulated angles, with a difference of less than 0.5 dB between the 0° and 30°. It is notable, that grating lobes appear at higher frequencies for oblique incidence (i.e. $\theta > 10°$).

IV. EXPERIMENTAL SETUP

The frequency response of the structure was obtained experimentally using a free space microwave anechoic chamber as seen in Fig. 13. The reflection and transmission response was obtained using a HP8510C Vector Network Analyzer (VNA). The sample was centrally positioned on a polystyrene foam block, suspended equidistantly between two horn antennas with distance, D_1, of 800 mm ensuring that the majority of the main beam is intercepted by the sample and that the measurements were made in using linearly polarized radiation. Multi octave horn antennas (A-INFO/LB-75180-20) were used in the measurements, with an average 20 dBi gain and −30 dB cross-polar isolation over the investigated frequency range.

Response type calibrations were conducted in the frequency domain and used to isolate the response of the sample in MATLAB without the need to calibrate the system prior to measurement. The reflection response due to the sample, S_{11} was found

$$S_{11} = \frac{M - I}{R - I} \tag{2}$$

where, M is the measured reflection response of the sample, I is the isolation measurement with no sample present and R is the reflected measurement of a conductive plate the same size as the sample. Similarly, the co-polarized and cross-polarized transmission response due to the sample, S_{21} was found

$$S_{21} = \frac{M - D}{C - D} \tag{3}$$

where, M is the measured transmission response of the sample, D is the diffracted measurement of a conductive plate the same size as the sample and C is the free space or calibration measurement where no sample is present. The co-polarized measurements were conducted with the transmitting and receiving antennas directed at each other in the same orientation (X-Polarization), which aligned with the polarization of the surface on the transmitter side. The cross-polarized measurements were conducted with the antennas directed at each other with the receiving antenna (Y-Polarization) in an orthogonal polarization with respect to the transmitting antenna (X-Polarization), with the orientation of the sample being unchanged. The measured results were time gated using a Kaiser-Bessel window with $\alpha = 1.92$ to identify and remove stray reflections within the system [24].

V. EXPERIMENTAL VERIFIACTION

The simulated and measured results are presented in Fig. 14, and show good agreement. The simulated reflection possesses two distinct minimums at 8 GHz and 10.3 GHz, with a rejection bandwidth of 37.7%, whilst the measured results displayed minimums at 8.3GHz and 10.6GHz with a rejection bandwidth of 50.8%. The transmission results also show good agreement, where the co-polarized magnitude is below −10 dB and the cross-polarized magnitude was above −10 dB, at around −3 dB to −4 dB for both the simulated and measured cases. Both co-polarized results possessed two peaks within the operating range, with the simulated results showing more distinct peaks at 8.0 GHz and 10.4 GHz. The measured results also had two peaks at 8.2 GHz and 10.7 GHz, displaying minimal reflection across the operating range. In the cross-polarized simulated transmission results, a −6 dB bandwidth ranging from 7.2 GHz to 13.5 GHz is observed with a 61.1% bandwidth.

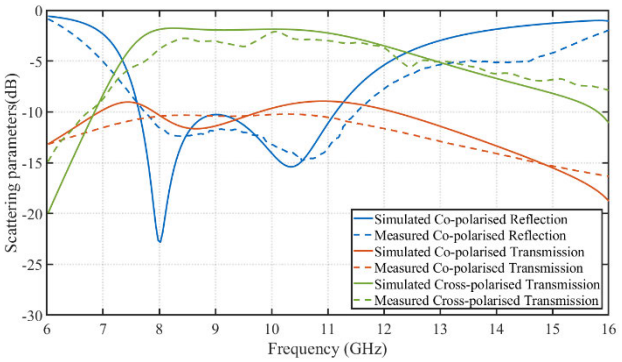

FIGURE 14. Simulated and measured response of the polarization rotating structure.

Similarly, the measured cross-polarized transmission results showed a −6 dB bandwidth ranging from 7.4 GHz to

TABLE 2. Comparison to existing polarization rotating designs.

	Substrate thickness	-6dB Transmission Bandwidth	Insertion loss (dB)	Flexibility
[10]	$0.12\lambda_0$	2.7%	0.4	N
[11]	$0.17\lambda_0$	4.1%	4	N
[12]	$0.18\lambda_0$	12.1%	0.2	N
[15]	$0.053\lambda_0$	15.0%	0.5	N
Proposed	$\mathbf{0.034\lambda_0}$	**60.0%**	**2.7**	**Y**

13.8 GHz with a 60.2% bandwidth. Insertion losses for both the simulated and measured results were around −2 dB to −3 dB and −3 dB to −4 dB respectively, across the operating range. Due to the structures reduced dielectric thickness and additional dielectric and conductive losses due to the materials used, the losses are larger than other reported designs. The differences between the simulated and measured results can be attributed to the minor misalignments and the properties of the materials such as the non-linear behavior of the dielectrics and conductive losses.

VI. CONCLUSION

In this paper, an ultra-thin broadband transmission FSS rotation polarizer has been presented. This structure uses coupling between rotated FSS layers to select, rotate and transmit the incoming polarization. A sweep of key design parameters along with their influence on the structures performance was also conducted, where the bandwidth and a low profile were prioritized. The fabricated surfaces were created using a laser engraving technique where, thin and flexible samples and showed good agreement between the experimental and simulated transmission response. Table. 2 compares this structures performance over previously proposed designs, highlighting its improvements consisting of its reduced profile, increased −6 dB cross polarized transmission bandwidth as well as its flexibility. Notably this increased bandwidth and reduced thickness comes at the price of a greater insertion loss. While these results were generated using a flat planar structure further work will consider the effect of bending of the structure on the performance.

REFERENCES

[1] B. A. Munk, *Frequency Selective Surfaces: Theory and Design*. New York, NY, USA: Wiley, 2000.

[2] J. C. Vardaxoglou, *Frequency Selective Surfaces: Analysis and Design*. Taunton, U.K.: Research Studies Press, 1997.

[3] P. Naseri, S. A. Matos, J. R. Costa, C. A. Fernades, and N. J. G. Fonseca, "Dual-band dual-linear-to-circular polarization converter in transmission mode application to *K*/*Ka* band satellite communications," *IEEE Trans. Antennas Propag.*, vol. 66, no. 12, pp. 7128–7137, Dec. 2018.

[4] M. Fartookzadeh and S. H. M. Armaki, "Enhancement of dual-band reflection-mode circular polarizers using dual-layer rectangular frequency selective surfaces," *IEEE Trans. Antennas Propag.*, vol. 64, no. 10, pp. 4570–4575, Oct. 2016.

[5] F. Samadi, M. Akbari, S. Zarbakhsh, R. Chaharmir, and A. Sebak, "High efficient linear polariser using FSS structure," *IET Microw., Antennas Propag.*, vol. 13, no. 1, pp. 88–91, Jan. 2019.

[6] I. L. Morrow and P. Thomas, "Compact frequency selective surface for polarisation transform," *Electron. Lett.*, vol. 50, no. 2, pp. 64–65, Jan. 2014.

[7] G. I. Kiani and V. Dyadyuk, "Quarter-wave plate polariser based on frequency selective surface," in *Proc. 40th Eur. Microw. Conf.*, Sep. 2010, pp. 1361–1364.

[8] Y. Li, J. Zhang, S. Qu, J. Wang, L. Zheng, A. Zhang, and Z. Xu, "Ultra-broadband linearly polarisation manipulation metamaterial," *Electron. Lett.*, vol. 50, no. 23, pp. 1658–1660, Nov. 2014.

[9] T. Zhong, H. Zhang, R. Wu, and X. L. Min, "A frequency selective surface with polarization rotation based on substrate integrated waveguide," *Prog. Electromagn. Res. Lett.*, vol. 60, pp. 121–125, May 2016.

[10] Z. Yu, Z.-X. Shen, and Y.-J. Feng, "Frequency-selective microwave polarization rotator using substrate-integrated waveguide cavities," *Chin. Phys. B*, vol. 23, no. 3, Jan. 2016, Art. no. 034101.

[11] S. A. Winkler, W. Hong, M. Bozzi, and K. Wu, "A novel polarization rotating frequency selective surface based on substrate integrated waveguide technology," in *Proc. 39th Eur. Microw. Conf.*, Oct. 2009, pp. 260–263.

[12] X. Liu, X. Cao, J. Yu, X. Chen, Y. Yao, L. Qi, Z. Chen, and J. Zhou, "Polarization rotator of arbitrary angle based on simple slot-array," *AIP Adv.*, vol. 5, no. 12, Dec. 2015, Art. no. 127142.

[13] M. H. Abad and N. Behdad, "A broadband, circular-polarization selective surface," *J. Appl. Phys.*, vol. 119, Jun. 2016, Art. no. 244901.

[14] R. Sivasamy and M. Kanagasabai, "Design and fabrication of flexible FSS polarizer," *Int. J. RF Microw. Comput.-Aided Eng.*, vol. 30, no. 1, Jan. 2020, Art. no. e22002.

[15] D. S. Wang, P. Zhao, and C. H. Chan, "Design and analysis of a high-selectivity frequency-selective surface at 60 GHz," *IEEE Trans. Microw. Theory Techn.*, vol. 64, no. 6, pp. 1694–1703, Jun. 2016.

[16] K. Karkkainen and M. Stuchly, "Frequency selective surface as a polarization transformer," *IEE Proc., Microw., Antennas Propag.*, vol. 149, pp. 248–252, Oct./Dec. 2002.

[17] R. Pous and D. M. Pozar, "A frequency-selective surface using aperture-coupled microstrip patches," *IEEE Trans. Antennas Propag.*, vol. 39, no. 12, pp. 1763–1769, Dec. 1991.

[18] M. Saikia, S. Ghosh, and K. V. Srivastava, "Design and analysis of ultrathin polarization rotating frequency selective surface using V-shaped slots," *IEEE Antennas Wireless Propag. Lett.*, vol. 16, pp. 2022–2025, Nov. 2017.

[19] T.-K. Wu, "Meander-line polarizer for arbitrary rotation of linear polarization," *IEEE Microw. Guided Wave Lett.*, vol. 4, no. 6, pp. 199–201, Jun. 1994.

[20] B. Li and Z. Shen, "Three-dimensional bandpass frequency-selective structures with multiple transmission zeros," *IEEE Trans. Microw. Theory Techn.*, vol. 61, no. 10, pp. 3578–3589, Oct. 2013.

[21] G. Q. Luo, W. Hong, Q. H. Lai, K. Wu, and L. L. Sun, "Design and experimental verification of compact frequency-selective surface with quasi-elliptic bandpass response," *IEEE Trans. Microw. Theory Techn.*, vol. 55, no. 12, pp. 2481–2487, Dec. 2007.

[22] N. Littman, G. O. Steven, A. Galehdar, H. G. Espinosa, and D. V. Thiel, "Fabrication of RF elements on thin plastic substrate using laser engraving technique," *Flexible Printed Electron.*, vol. 6, no. 2, May 2021, Art. no. 025002.

[23] A. R. Amiet, "Free space permittivity and permeability measurements at microwave frequencies," Ph.D. dissertation, Dept. Electr. Comput. Syst. Eng., Monash Univ., Clayton, VIC, Australia, 2003.

[24] R. F. Harrington, "Some theorems and concepts," in *Time-Harmonic Electromagnetic Fields*. New York, NY, USA: Wiley, 1961.

NICKOLAS M. LITTMAN (Student Member, IEEE) received the B.Eng. degree (Hons.) in microelectronic engineering from Griffith University, Brisbane, QLD, Australia, in 2017, where he is currently pursuing the Ph.D. degree with the Griffith School of Engineering.

His current research interests include design and modeling of frequency selective surface (FSS) and metamaterials with novel electromagnetic behavior, radar absorbing materials, and antenna measurements.

STEVEN G. O'KEEFE received the B.Sc. degree in physics, mathematics, and electronics from Griffith University, Brisbane, QLD, Australia, in 1985, the B.Sc. degree (Hons.) in electronics and the M.Sc. degree in biomedical electronics from La Trobe University, Melbourne, VIC, Australia, in 1986 and 1990, respectively, and the Ph.D. degree in geophysical electromagnetics from Griffith University, in 1996.

He is currently an Associate Professor and the Head of electronic engineering with the Griffith School of Engineering and Built Environment, Griffith University. His current research interests include compact mobile antenna design and electromagnetic geophysics.

AMIR GALEHDAR (Member, IEEE) received the B.Eng. degree in telecommunication engineering from K. N. Toosi University of Technology, in 2002, and the M.Eng. (Hons.) and Ph.D. degrees in antenna development for RFID applications from Griffith University, Brisbane, Australia, in 2005 and 2009, respectively. He held a Research Fellow position at RMIT University, Melbourne, Australia, for three years, where he was awarded with the Defence Materials Technology Centre's Early Career Award for his contribution to defense, in 2012. He joined the Electromagnetic Signature Control Group, Defence Science and Technology Organisation, in 2012, where his main responsibility is to reduce radar signature of Australian defence force platforms. His research interests include radar absorbing materials, multi-functional platforms, load bearing conformal carbon fiber reinforced polymers (CFRP) antennas, small antennas, and radio frequency identification (RFID) antennas. He was awarded with DST Group's Outstanding Early Career Achiever award, in 2016.

HUGO G. ESPINOSA (Senior Member, IEEE) received the B.Eng. degree in electronics and telecommunications engineering from Monterrey Institute of Technology and Higher Education, State of Mexico, Mexico, in 1998, the M.Eng. degree in electrical engineering from the University of Sao Paulo, Sao Paulo, Brazil, in 2002, and the Ph.D. degree *(summa cum laude)* in electrical engineering from the Technical University of Catalonia, Barcelona, Spain, in 2008. He has been a Visiting Researcher with the Federal Polytechnic School of Lausanne, Lausanne, Switzerland, and a Postdoctoral Fellow with the School of Electrical Engineering, Tel Aviv University, Tel Aviv, Israel. Since 2011, he has been with the School of Engineering and Built Environment, Griffith University, Brisbane, QLD, Australia, where he is currently a Senior Lecturer in electronic engineering. His research interests include computational electromagnetics, antennas and propagation, wireless sensor networks, inertial sensors, and wearable sensor technology for human monitoring.

DAVID V. THIEL (Life Senior Member, IEEE) received the bachelor's degree in physics and applied mathematics from The University of Adelaide, Adelaide, SA, Australia, and the M.S. and Ph.D. degrees from James Cook University, Townsville, QLD, Australia.

He is currently a Professor with the School of Engineering and Built Environment and the Director of the Griffith University Sport Technology (GUST) Laboratories, Griffith University, Brisbane, QLD, Australia. He authored the book *Research Methods for Engineers* (Cambridge, U.K.: Cambridge University Press, 2014), and coauthored a book on *Switched Parasitic Antennas for Cellular Communications* (Norwood, MA, USA: Artech House, 2002). He has authored six book chapters, over 150 journal articles, and coauthored more than nine patent applications. His research interests include electromagnetic geophysics, sensor development, electronics systems design and manufacture, antenna development for wireless sensor networks, environmental sustainability in electronics manufacturing, sports engineering, and mining engineering.

Prof. Thiel is a fellow of the Institution of Engineers, Australia, and a Chartered Professional Engineer in Australia.